Article

Wettability Alteration of a Thiolene-Based Polymer (NOA81): Surface Characterization and Fabrication Techniques

Mahtab Masouminia, Kari Dalnoki-Veress, Charles-François de Lannoy, and Benzhong Zhao*
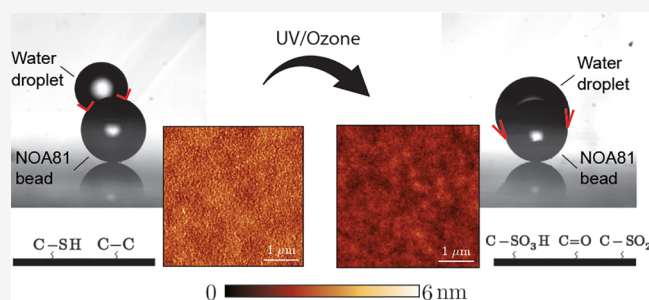
Read Online

ACCESS | Metrics & More | Article Recommendations | Supporting Information

ABSTRACT: Wettability plays a significant role in controlling multiphase flow in porous media for many industrial applications, including geologic carbon dioxide sequestration, enhanced oil recovery, and fuel cells. Microfluidics is a powerful tool to study the complexities of interfacial phenomena involved in multiphase flow in well-controlled geometries. Recently, the thiolene-based polymer called NOA81 emerged as an ideal material in the fabrication of microfluidic devices, since it combines the versatility of conventional soft photolithography with a wide range of achievable wettability conditions. Specifically, the wettability of NOA81 can be continuously tuned through exposure to UV−ozone. Despite its growing popularity, the exact physical and chemical mechanisms behind the wettability alteration have not been fully characterized. Here, we apply different characterization techniques, including contact angle measurements, X-ray photoelectron spectroscopy (XPS), and atomic force microscopy (AFM) to investigate the impact of UV−ozone on the chemical and physical properties of NOA81 surfaces. We find that UV−ozone exposure increases the oxygen-containing polar functional groups, which enhances the surface energy and hydrophilicity of NOA81. Additionally, our AFM measurements show that spin-coated NOA81 surfaces have a roughness less than a nanometer, which is further reduced after UV−ozone exposure. Lastly, we extend NOA81 use cases by creating (i) 2D surface with controlled wettability gradient and (ii) a 3D column packed with monodisperse NOA81 beads of controlled size and wettability.

INTRODUCTION

Fluid−fluid displacement in small, confined geometries is strongly influenced by the relative affinity of the surrounding solid for the different fluids (i.e., wettability) .[1−3] Wettability at the small-scale has important implications in a variety of large-scale natural and industrial processes, including vadose zone hydrology,[4−6] enhanced oil recovery,[7,8] geologic carbon and hydrogen storage,[9,10] and electrochemical energy conversion and storage.[11,12] Microfluidic devices offer a powerful experimental platform to study the impact of wettability on fluid−fluid displacement, since they allow for direct visualization of the fluid interfaces and they can be fabricated with controllable geometries.[13−16]

Different techniques have been introduced to tune the wettability condition of microfluidic experiments, which include the use of different fluid−fluid pairs,[17] chemical vapor deposition (CVD) or liquid solution deposition of silane molecules,[18,19] coating silica surfaces with Aquaphobe-CM and hexane solution under high temperature and high pressure conditions,[20] oxidization of polydimethylsiloxane (PDMS) surfaces via either corona discharge[21] or oxygen plasma[22] treatment, and coating PDMS surfaces with a sol−gel layer that is functionalized with fluorinated and photoreactive silanes.[23,24] Recently, the polymer called NOA81 (Norland Products, USA) has emerged as an alternative material for

fabricating microfluidic devices with controlled wettability conditions.[25−28] NOA81 is a thiolene-based photocurable resin that enables patterning of submicrometer-size features via soft imprint lithography.[29] In addition to the many positive attributes including solvent resistance, biocompatibility, and high elastic modulus,[30,31] NOA81 offers the following advantages when it comes to wettability alteration: (i) its wettability can be continuously tuned and controlled by varying the duration of UV−ozone exposure.[25] Specifically, the wettability as measured by the contact angle θ of water in silicone oil varies over a wide range ($\theta = 7-120°$).[26] This wettability alteration is especially desirable since both water and silicone oil are commonly used and well characterized analog liquids in studies of capillarity and interfacial phenomena. Furthermore, the viscosity ratio between silicone oil and water can be varied significantly without appreciable

change in their interfacial tension.[32] (ii) The change in wettability is stable over a time scale of many days.[25]

Despite the growing popularity of NOA81 in microfluidic studies (e.g., refs 26 and 33−39), the physical and chemical mechanisms behind the UV−ozone-induced wettability alteration have not been characterized. Our work aims to fill this knowledge gap. To this end, we first create a highly uniform NOA81 thin film via spin coating on a silicon wafer. We then employ characterization techniques including contact angle, X-ray photoelectron spectroscopy (XPS), and atomic force microscopy (AFM) measurements to investigate changes to the NOA81 surface as a result of UV−ozone treatment. Our analyses show that wettability alteration on NOA81 surfaces arises as a result of the emergence of polar, oxygen-containing functional groups after UV−ozone exposure. Finally, we extend the potential use cases for NOA81 by introducing procedures to generate (i) NOA81 surfaces with controlled wettability gradients and (ii) monodisperse NOA81 beads with controlled size and wettability.

■ SURFACE FABRICATION

A survey of the literature shows that existing NOA81 surfaces in microfluidics applications are fabricated via replica molding. In this method, NOA81 is sandwiched between a flat surface and a mold (typically made of PDMS) in the negative shape of the desired micropattern before the NOA81 is cured.[25−27,29,35] To generate a flat NOA81 surface via replica molding, we first fabricate a flat PDMS (Sylgard 184, Dow Corning, USA) substrate that is cured on a silicon wafer. We then sandwich a drop of NOA81 between a silicon wafer and the flat PDMS substrate, separated by 100 μm thick precision shims. After curing the NOA81 with 365 nm UV light for 10 s, we peel off the PDMS substrate to reveal the NOA81 surface (Figure 1A). We expose the NOA81 surface to UV (365 nm) for an additional 20 s after PDMS removal to cure the ultrathin superficial layer of NOA81.[29] We measure the topography and roughness of the NOA81 surface with an atomic force microscope (MultiMode 8-HR, Bruker, USA) with a scan area of $15 \times 15 \ \mu m^2$. We find that the NOA81 surface made by replica molding has a root-mean-square (RMS) roughness of ∼1.32 nm, with a correlation length of ∼0.95 μm (Figure 1C).

We then create a thin film of NOA81 on a silicon wafer by spin-coating. To avoid dewetting, the silicon wafer is first treated in an oxygen plasma asher for 1 min (model PT7150, Bio-Rad, USA); NOA81 thin films spin-coated on untreated silicon wafers are unstable at ambient temperature (20 °C) and they undergo spinodal dewetting. We achieve a stable NOA81 thin film at spin speed of 4000 rpm for 30 s, which is then cured with 365 nm UV light for 10 s (Figure 1B). We perform ellipsometry using a spectroscopic ellipsometer (model M-2000, J. A. Woolam, USA) to determine the thickness of the spin-coated films. Three different spots are measured at five different incidence angles, 55°, 60°, 65°, 70°, and 75°. The measured thickness of the NOA81 film is 6.05 μm. AFM measurement of the spin-coated NOA81 surface reveals that it has an RMS roughness of ∼0.6 nm, with a correlation length of ∼0.6 μm (Figure 1D). Therefore, spin-coating generates a smoother NOA81 surface at the nanoscale compared to replica molding, and we use the spin-coated NOA81 surface in charaterizations discussed in subsequent sections.
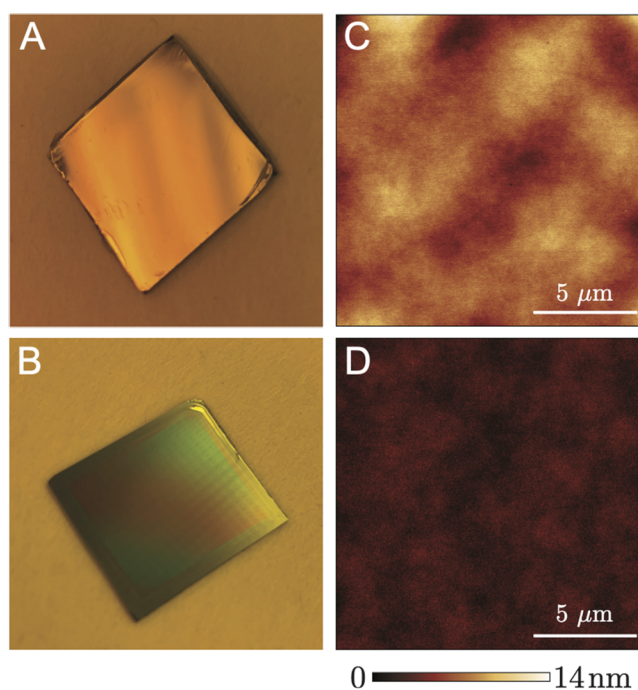

Figure 1. (A) Thin film of NOA81 cured on a 1 in. × 1 in. silicon wafer created by PDMS replica molding. The thickness of the NOA81 is 100 μm. (B) Thin film of NOA81 cured on a 1 in. × 1 in. silicon wafer created by spin coating. The thickness of the NOA81 is ∼6.05 μm. (C) AFM surface roughness measurements of the NOA81 film created by PDMS replica molding. (D) AFM surface roughness measurements of the NOA81 film created by spin coating. Both methods generate smooth coatings with roughness less than 14 nm, though spin coating attains a significantly more homogeneous film.

■ SURFACE PROPERTY CHANGE DUE TO UV−OZONE EXPOSURE

Contact Angle Characterization. NOA81 surface is known to become more hydrophilic after exposure to UV−ozone treatment. Levaché et al.[25] characterized the UV−ozone induced contact angle change in NOA81 surface made by replica molding for water-in-air and water-in-hexadecane oil systems. Here, we treat the spin-coated NOA81 surfaces for different durations in a UV−ozone cleaner (model T0606B, UVOCS, USA), which has a low-pressure quartz−mercury vapor lamp that generates UV emissions in the 185 and 254 nm range. The intensity of 254 nm UV is 10 mW/cm^2 1 inch away from the source.

We characterize the wettability of the surfaces by measuring the static contact angle of water using a contact angle goniometer immediately after UV−ozone exposure. The measurements are conducted for both water-in-air and water-in-silicone oil (MilliporeSigma, USA) systems. The water-in-air contact angle measurements are repeated at six different spots on each sample (Figure 2). The change in NOA81 surface wettability as a function of UV−ozone exposure can be described by an exponential function:

$$\theta = (\theta_1 - \theta_2) \exp(-t/\tau) + \theta_2 \qquad (1)$$

where θ is the static contact angle of water, t is the exposure duration in minutes, θ_1 is the initial contact angle, θ_2 is the final contact angle, and τ is a time constant. We find $\theta_1 = 65°$, $\theta_2 = 10°$, $\tau = 5$ min for the water-in-air system; $\theta_1 = 103°$, $\theta_2 = 17°$, $\tau = 8$ min for the water-in-silicone oil system.
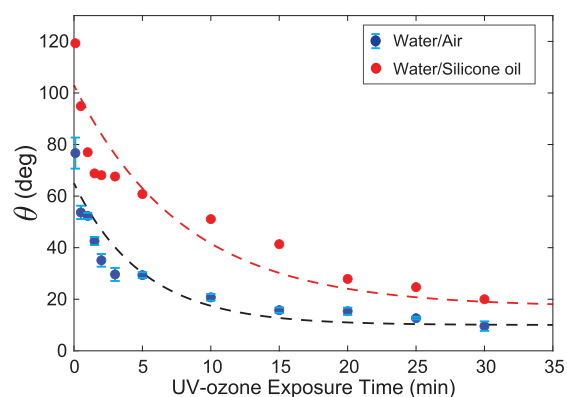
Figure 2. Static contact angle θ of water on spin-coated NOA81 surfaces as a function of UV−ozone exposure time for two different ambient fluids: air (blue circles) and silicone oil (red circles). The contact angle of the NOA81 surface decreases with increasing UV−ozone exposure time in the presence of both ambient fluids. The dashed lines represent the exponential fit (eq 1), while the error bars represent the standard deviation of the contact angle measurements for water-in-air system.

Surface Chemistry Characterization. The dramatic change in NOA81's wettability after UV−ozone exposure suggests a corresponding change in its surface chemistry. We characterize the surface chemistry of untreated and UV−ozone treated NOA81 surfaces with XPS, which provides quantitative information on the elemental composition, as well as chemical composition of the surface.[40] Additionally, we perform XPS characterization of NOA81 samples treated with ozone alone to elucidate the impact of UV on surface chemistry modification. Details of the experimental setup for ozone-treated samples are included in the Supporting Information. The XPS analyzer (model PHI Quantera II, Physical Electronics, USA) is equipped with a monochromatic Al Kα X-ray (1486.6 eV) source and operated under ultrahigh vacuum ($\sim10^{-9}$ Torr) at a photoelectron takeoff angle of 45°. We use a pass energy of 224 eV with an energy step of 0.8 eV to obtain the full spectrum in the binding energy range between 0 and 1100 eV. We additionally use a pass energy of 26 eV with an energy step of 0.1 eV to acquire high-resolution spectra. All spectra are calibrated with reference to the C 1s spectrum at 284.8 eV and analyzed using Gaussian−Lorentzian peak deconvolution along with Shirley background reduction using MultiPak Spectrum software.[41] The XPS survey scans are collected at three different points for each sample. The full spectrum of untreated, ozone-treated, and UV−ozone-treated samples are presented in Figure S2 of the Supporting Information. The XPS survey scans confirm the presence of the elements C (carbon), S (sulfur), O (oxygen), and N (nitrogen) as C 1s, O 2s, O 1s, S 2p, S 2s, and N 1s peaks. S 2p, C 1s, and O 1s peaks are further analyzed in detail to identify chemical changes due to ozone and UV−ozone treatment.

Figure 3 shows the high-resolution spectra of NOA81 film before treatment (first row), after 5 min (second row) and 30 min (third row) of ozone treatment, as well as after 5 min (fourth row) and 30 min (last row) of UV−ozone treatment. Additional high-resolution spectra for NOA81 film after 1 min ozone and 1 min UV−ozone exposure are presented in Figure S3 of the Supporting Information. The shifts in the energy of XPS high-resolution spectra indicate changes in surface functional groups as a result of UV−ozone treatment. The S

2p spectrum of the untreated NOA81 surface shows two peaks at binding energies of 162.6−163.2 eV and 163.6−164.5 eV, which correspond to sulfide (C−S−C) slightly polar functional group and thiol (C−S−H) nonpolar functional group. After UV−ozone treatment, we observe the emergence of two oxidized sulfur species, which correspond to sulfone (C−SO$_2$−C) at a binding energy of 167.3−168.1 eV and sulfonate (C−SO$_3$−H) at a binding energy of 168.5−169.4 eV.[42−45] Sulfone and sulfonate are absent on NOA81 surfaces treated with ozone alone, demonstrating that UV is essential in creating the oxidized sulfur species. The C 1s spectrum of the untreated NOA81 surface has three peaks at binding energies of 284.6−284.8 eV, 285.9−286 eV, and 288.6−289 eV corresponding to hydrocarbon (C−C/C−H) nonpolar groups, ether (C−O), and carboxyl (O−C=O) polar functional groups. After UV−ozone treatment, we observe the emergence of a new peak at a binding energy of 287.6−287.7 eV, which is most likely carbonyl (C=O) polar functional group.[46,47] However, we do not see the appearance of carbonyl group on NOA81 surfaces treated with ozone alone, demonstrating the importance of UV in its creation. The O 1s spectrum of the untreated NOA81 surface are fitted with two contributions, arising from C−O at 532.8−533.2 eV and C=O at 531.4−531.9 eV binding energy.[48,49] The shift in XPS peaks after ozone/UV−ozone treatment is less dramatic in the O 1s spectrum compared to the S 2p and C 1s spectra. However, we find that the ratio of carbon−oxygen double bonds to carbon−oxygen single bonds is higher on NOA81 samples that have been exposed to UV−ozone treatment compared to those treated with ozone alone, which is consistent with UV−ozone induced growth of carbonyl (C=O) functional groups observed in the C 1s spectrum.

Contact angle measurement on NOA81 surfaces treated with ozone alone shows that surface hydrophilicity enhancement is much less dramatic compared to surfaces treated with UV−ozone (Figure S4 of the Supporting Information). These results demonstrate that high-energy UV irradiation plays a fundamental role in forming the polar functional groups and wettability alteration of NOA81 surfaces and that ozone alone is not sufficient to achieve a significant increase in hydrophilicity. Mechanistically, the high-energy UV light of a quartz−mercury lamp continually generates and destroys ozone to yield a steady-state concentration of strongly oxidizing atomic oxygen. High-energy UV is known to lead to the cracking of near-surface bonds of plastics, which, together with oxidative stress, facilitates the formation of oxygen-containing functional groups.[50]

Surface Topology Characterization. We characterize the physical changes to the NOA81 surface as a result of UV−ozone treatment. Specifically, AFM measurements demonstrate that UV−ozone exposure makes NOA81 surfaces smoother, though the effect is quite small (Figure 4A,B). The untreated NOA81 has an RMS roughness of 0.61 nm with a correlation length of 19.47 nm, while the NOA81 surface that has been exposed to UV−ozone for 30 min has an RMS of 0.37 nm and a correlation length of 63.23 nm. Additionally, ellipsometry measurements show that NOA81 film thickness decreases monotonically with increasing UV−ozone treatment time; the film thickness decreases by $\sim$300 nm after 30 min UV−ozone exposure (Figure 4C).
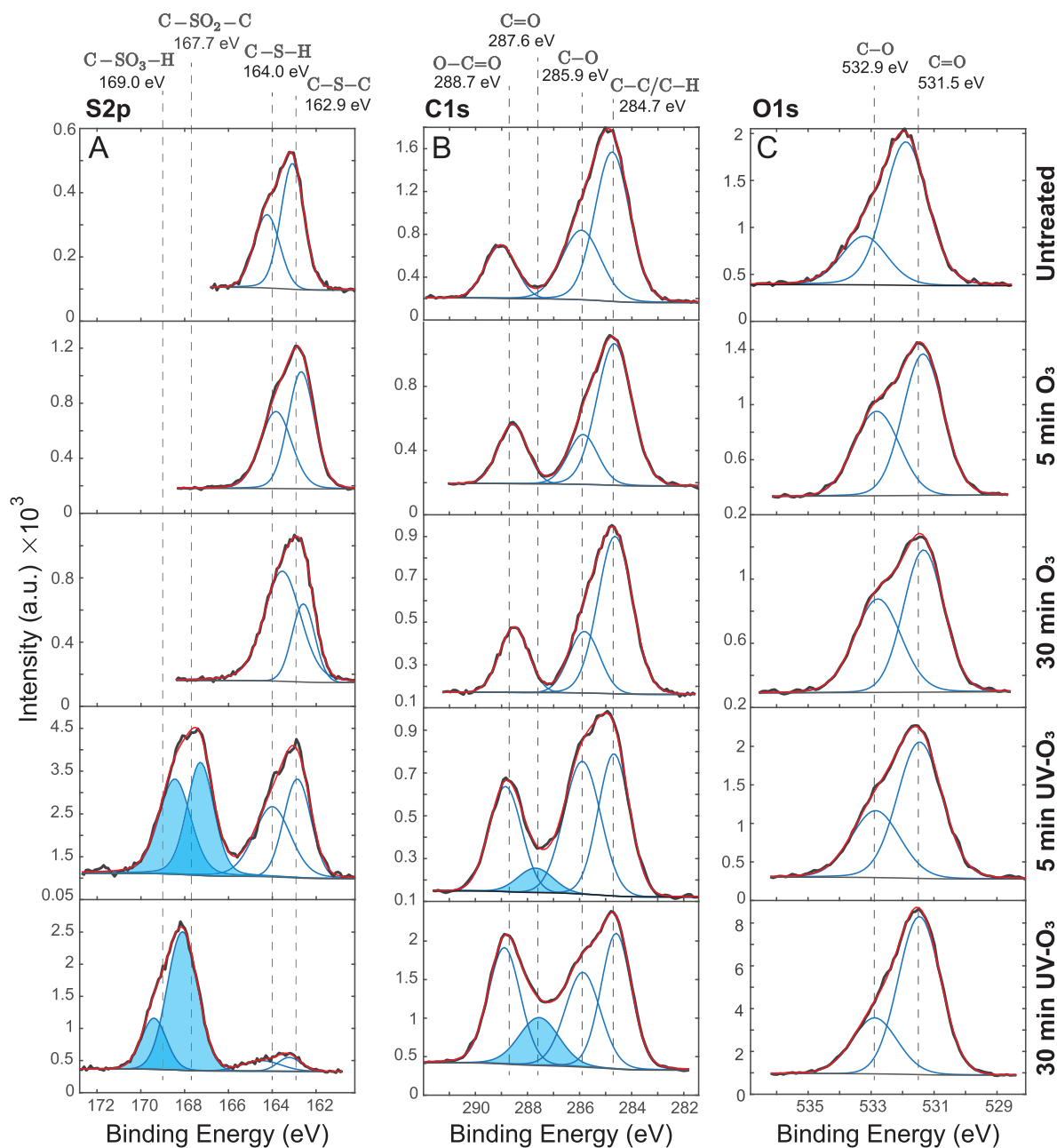
Figure 3. We characterize the surface chemical compositions of untreated, 5 and 30 min ozone-treated, and 5 and 30 min UV−ozone-treated NOA81 films via XPS. The high-resolution spectra of S 2p (column A), C 1s (column B), and O 1s (column C) are shown for each sample. The highlighted peaks correspond to the emergence of sulfonate, sulfone, and carbonyl polar functional groups after UV−ozone treatment.
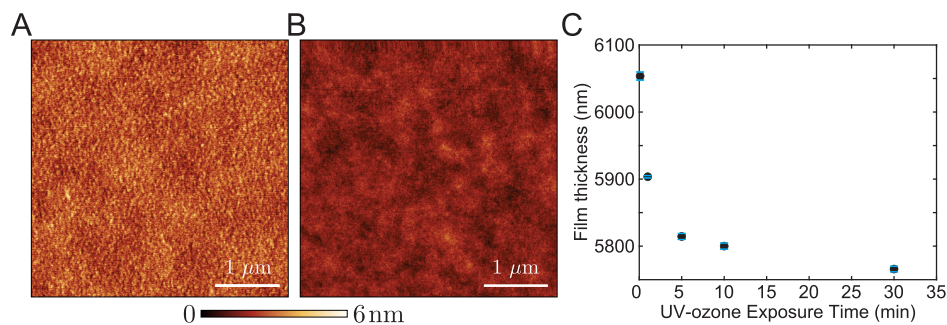

Figure 4. AFM surface morphologies of the spin-coated NOA81 film (A) not exposed to UV−ozone and (B) exposed to UV−ozone for 30 min demonstrate that UV−ozone exposure reduces the roughness of the NOA81 film. (C) The NOA81 film thickness decreases monotonically with increasing UV−ozone exposure.
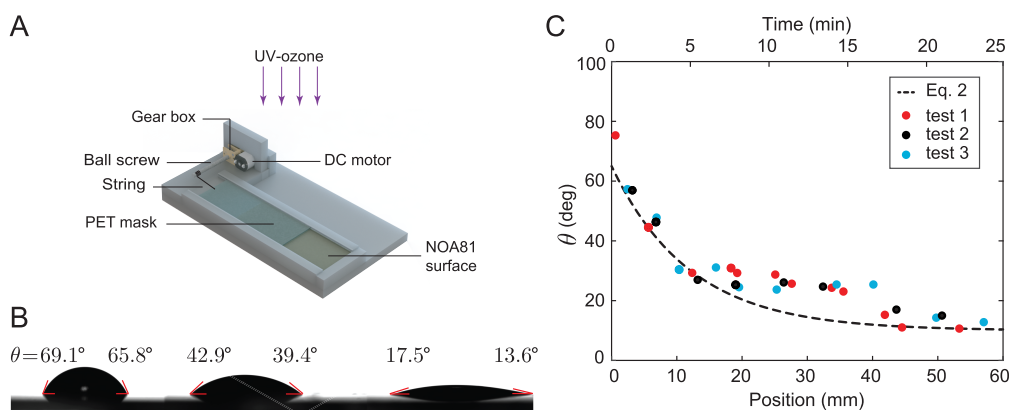
Figure 5. (A) Schematic of the fabrication platform to generate wettability gradients on NOA81 surfaces. We control the amount of high-energy UV exposure on the NOA81 surface via an overlying UV-blocking PET mask that is gradually retracted by a DC motor. (B) Left and right contact angles of three water droplets placed along a NOA81 surface with a wettability gradient in the presence of air. (C) The measured contact angles along the wettability gradient surface (circles) agree with predictions of eq 2 (dashed line).
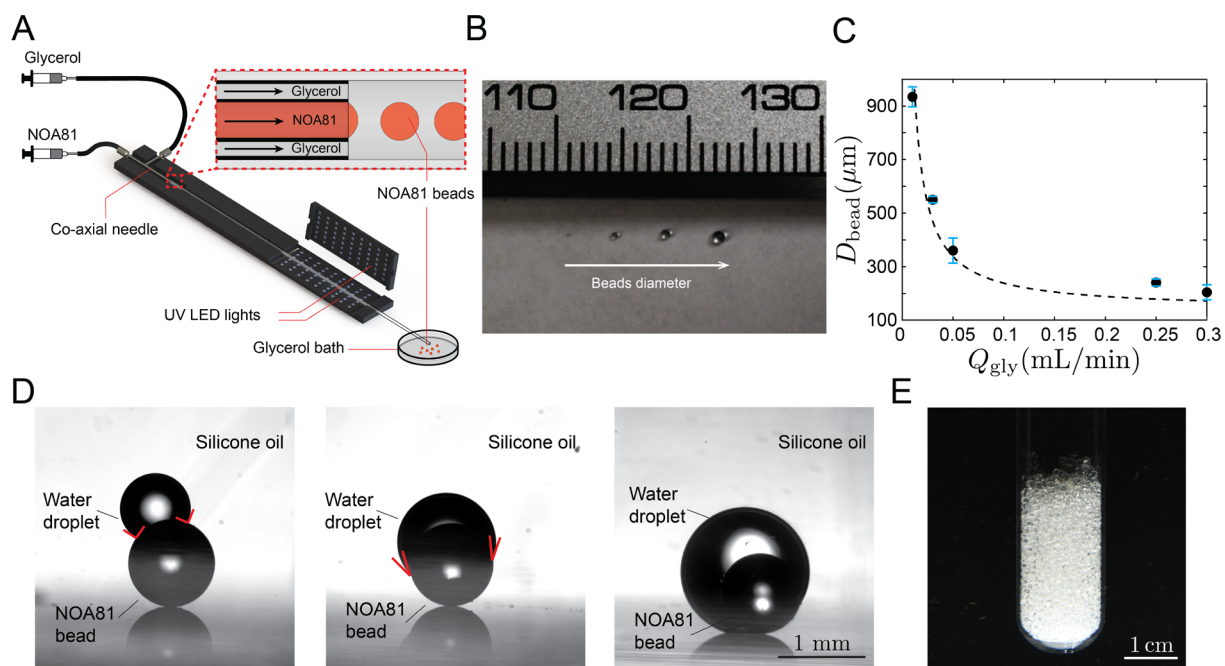

Figure 6. (A) Schematic of the microfluidic platform for generating NOA81 sphere beads with controlled size and wettability. We use a coaxial needle as a droplet generator to form the NOA81 droplets. Glycerol is the continuous phase, and NOA81 is the dispersed phase. UV LED lights downstream cure the NOA81 droplets. (B) Pictures of NOA81 beads with different diameters (220, 500, 715, and 930 μm from left to right). (C) The beads' diameter (D_{bead}) as a function of glycerol flow rate (Q_{gly}) at a fixed NOA81 flow rate ($Q_{NOA81} = 0.0001$ mL/min). (D) Left: The contact angle of water on an untreated NOA81 bead in a bath of silicone oil is 92°. Middle: The contact angle of water in silicone oil on a NOA81 bead that has been exposed to 30 min of UV−ozone is 26°. Right: The NOA81 bead that has been exposed to 2 h of UV−ozone becomes fully encapsulated by the water drop. (E) Column packed with monodisperse NOA81 beads.

■ EXTENSION OF USE CASES

Surface with Controlled Wettability Gradient. Wettability gradient is a common occurrence in many natural and industrial processes; for example, the diffusion of biosurfactants produced by bacteria can locally make soil particles more water-wet,[51] and the dispersion of asphaltenes can locally make reservoir rocks more oil-wet.[52] In the context of lab-on-a-chip technology, wettability gradients have been extensively utilized in the past two decades for the spontaneous and directional transport of liquid droplets in analytical chemistry and bioassay applications.[53−55]

Here, we introduce a fabrication technique to generate wettability gradients on NOA81 surfaces. Specifically, we take advantage of the property that NOA81 becomes more hydrophilic with increasing exposure to UV−ozone (Figure 2) via the application of a UV-blocking polyethylene terephthalate (PET) mask. The PET mask is placed on top of the NOA81 surface and attached to a direct current (DC) motor via a taut string on one side. The motor gradually pulls back the mask along a track at a constant velocity, exposing the underlying NOA81 surface to UV−ozone (Figure 5A). The cumulative exposure of the NOA81 surface varies along the travel direction of the mask, which results in a spatial wettability gradient:

$$\theta = (\theta_1 - \theta_2) \exp\left(-\frac{x}{v\tau}\right) + \theta_2 \tag{2}$$

where θ_1, θ_2, τ are the fitting parameters described in eq 1, v is the velocity of the PET mask, and $x \in [0, L]$ is the position along the substrate of length L. We generate a wettability gradient on an $L = 60$ mm long NOA81-coated microscope slide with $v = 2.4$ mm/min (Figure 5), which agrees well with the contact angle distribution predicted by eq 2. We note that one can design and achieve different types of wettability gradients by employing a varying mask velocity in time, which can be accomplished by connecting the DC motor to a programmable microcontroller (e.g., Arduino Nano).

Spherical Beads with Controlled Wettability and Size. NOA81 micromodels in the existing literature have been constructed in Hele-Shaw-type geometries (e.g., refs 26, 36, 38, and 39), where fluid flow takes place between two parallel flat surfaces separated by a small gap. An alternative method of creating micromodels is by packing spherical beads between parallel plates[56−59] or in a tube.[60−62] This type of micromodel has made fundamental contributions to our understanding of multiphase flow in porous media.

Here, we introduce a simple microfluidic platform for generating NOA81 beads with controlled size and wettability. Upstream of the microfluidic platform consists of a coaxial needle (ramé-hart, USA) connected to a Tygon tubing. We operate the coaxial needle in a coflow manner by injecting NOA81 through the smaller inner needle and glycerol (Sigma-Aldrich, USA) through the larger outer needle. In this setup, the less viscous NOA81 ($\mu_{NOA81} = 300$ mPa·s) forms a jet that penetrates into the more viscous glycerol ($\mu_{glycerol} = 648$ mPa·s). The jet of NOA81 becomes unstable and breaks into drops due to the Rayleigh−Plateau instability (Figure 6A and Movie S1) .[63,64] Downstream of the microfluidic platform consists of a chamber lined with UV LED lights, which cure the NOA81 droplets as they pass through. The cured NOA81 beads are collected, rinsed with deionized water, and dried with nitrogen gas. The drop size is controlled by the injection rates of NOA81 and glycerol. We use a coaxial needle with an inner needle with inner diameter ID = 140 μm and outer diameter OD = 305 μm and external needle with inner diameter ID = 584 μm and outer diameter OD = 889 μm to achieve monodisperse NOA81 beads whose diameters range between 212 and 934 μm (Figure 6B). For a given NOA81 flow rate (i.e., 0.0001 mL/min), the diameter of the generated bead is controlled by the glycerol flow rate Q_{gly} (Figure 6C)

$$D_{bead} = d_{needle}\left(1 + \frac{\alpha}{Q_{gly}}\right) \tag{3}$$

where D_{bead} is the diameter of the bead and d_{needle} is the inner diameter of the inner needle. $\alpha = 0.071$ mL/min is an empirically determined fitting parameter.

We characterize the wettability of the NOA81 beads by placing a small drop of water on the bead in a chamber filled with silicone oil, which yields a contact angle of 92° (Figure 6D, left, and Movie S2). To make the NOA81 beads more hydrophilic, we expose them to UV−ozone in a quartz glass Petri dish, since quartz glass has high transmission of the 185 and 254 nm UV light needed for wettability alteration. We attach a mirror to the bottom of the Petri dish, which reflects incident UV rays back toward the bottom of the beads. We wrap the sides of the Petri dish with reflective aluminum foil to further increase exposure uniformity. The contact angle of water in silicone oil on a NOA81 bead that has been exposed to UV−ozone for 30 min is 26° (Figure 6D, middle). Interestingly, the water drop is able to pick up the UV-treated NOA81 bead due to capillary adhesion (Movie S3). Further increasing the exposure time and the water drop volume triggers the total encapsulation of the NOA81 bead by the water (Figure 6D, right, and Movie S4). Finally, we demonstrate the scalability of the microfluidic platform by creating a column packed with NOA81 beads (Figure 6E), which could be used to investigate the impact of wettability and mixed-wettability on multiphase flow in truly 3D geometries.

CONCLUSIONS

We have presented a comprehensive investigation of the mechanisms behind wettability alteration on NOA81 surfaces as a result of UV−ozone. NOA81 is a thiolene-based photocurable polymer with growing popularity in microfluidics, since the wettability of NOA81 can be precisely tuned over a wide range of contact angles in both water−air and water−silicone oil systems (Figure 2). We characterize the surface chemistry of NOA81 via XPS measurements, which reveal the abundance of hydrophobic nonpolar functional groups (i.e., hydrocarbon and thiol) on untreated NOA81 surfaces and the formation of hydrophilic polar functional groups (i.e., carbonyl, sulfone, and sulfonate) on UV−ozone treated NOA81 surfaces (Figure 3). Critically, UV plays an essential role in the creation of the hydrophilic polar functional groups and that ozone treatment alone cannot achieve the same range of wettability alteration. Our AFM measurements reveal the highly smooth nature of spin-coated NOA81 surfaces (Figure 1), whose roughness further decreases after exposure to UV−ozone (Figure 4). Lastly, we demonstrate the ever-expanding potential of NOA81 in even more applications by designing fabrication systems to generate (i) a 2D surface with controlled wettability gradient (Figure 5) and (ii) monodisperse NOA81 beads with controlled size and wettability (Figure 6). These fabrication systems could enable experiments that further probe the impact of wettability on multiphase flow in porous media, including studies of immiscible viscous fingering with a spatial wettability gradient and propagation of corner flow in strong imbibition in model 3D geometries.

ASSOCIATED CONTENT

ⓢ Supporting Information

The Supporting Information is available free of charge at https://pubs.acs.org/doi/10.1021/acs.langmuir.2c02719.

> Description of the experimental setup to treat the NOA81 surface with ozone only, along with additional XPS and contact angle measurements (PDF)

> Movie S1 showing the generation of NOA81 droplets using a coaxial needle, where glycerol is the continuous phase and NOA81 is the dispersed phase (MOV)

> Movie S2 showing the contact angle measurement of water on an untreated NOA81 bead in a bath of silicone oil (MOV)

> Movie S3 showing the contact angle measurement of water in silicone oil on a NOA81 bead that has been exposed to 30 min of UV−ozone (MOV)

Movie S4 showing the total encapsulation of a NOA81 bead that has been exposed to 2 h of UV−ozone (MOV)

■ AUTHOR INFORMATION

Corresponding Author

Benzhong Zhao − *Department of Civil Engineering, McMaster University, Hamilton, Ontario L8S 4L8, Canada;* orcid.org/0000-0003-1136-9957; Email: robinzhao@mcmaster.ca

Authors

Mahtab Masouminia − *Department of Civil Engineering, McMaster University, Hamilton, Ontario L8S 4L8, Canada*

Kari Dalnoki-Veress − *Department of Physics & Astronomy, McMaster University, Hamilton, Ontario L8S 4L8, Canada*

Charles-François de Lannoy − *Department of Chemical Engineering, McMaster University, Hamilton, Ontario L8S 4L8, Canada*

Complete contact information is available at:
https://pubs.acs.org/10.1021/acs.langmuir.2c02719

Notes

The authors declare no competing financial interest.

■ ACKNOWLEDGMENTS

■ REFERENCES

(1) Cueto-Felgueroso, L.; Juanes, R. Macroscopic phase-field model of partial wetting: bubbles in a capillary tube. *Phys. Rev. Lett.* **2012**, *108*, 144502.

(2) Zhao, B.; Pahlavan, A. A.; Cueto-Felgueroso, L.; Juanes, R. Forced Wetting Transition and Bubble Pinch-Off in a Capillary Tube. *Phys. Rev. Lett.* **2018**, *120*, 144502.

(3) Zhao, B.; MacMinn, C. W.; Primkulov, B. K.; Chen, Y.; Valocchi, A. J.; Zhao, J.; Kang, Q.; Bruning, K.; McClure, J. E.; Miller, C. T.; et al. Comprehensive comparison of pore-scale models for multiphase flow in porous media. *Proc. Natl. Acad. Sci. U.S.A.* **2019**, *116*, 13799−13806.

(4) DeBano, L. F. The effect of hydrophobic substances on water movement in soil during infiltration. *Soil Sci. Soc. Am. J.* **1971**, *35*, 340−343.

(5) Hill, D. E.; Parlange, J.-Y. Wetting front instability in layered soils. *Soil Sci. Soc. Am. J.* **1972**, *36*, 697−702.

(6) Cueto-Felgueroso, L.; Juanes, R. Nonlocal Interface Dynamics and Pattern Formation in Gravity-Driven Unsaturated Flow through Porous Media. *Phys. Rev. Lett.* **2008**, *101*, 244504.

(7) Morrow, N.; Buckley, J. Improved oil recovery by low salinity waterflooding. *J. Pet. Technol.* **2011**, *63*, 106−112.

(8) Chen, P.; Mohanty, K. K. Surfactant-mediated spontaneous imbibition in carbonate rocks at harsh reservoir conditions. *Soc. Pet. Eng. J.* **2013**, *18*, 124−133.

(9) Chalbaud, C.; Robin, M.; Lombard, J. M.; Martin, F.; Egermann, P.; Bertin, H. Interfacial tension measurements and wettability evaluation for geological CO_2 storage. *Adv. Water Resour.* **2009**, *32*, 98−109.

(10) Iglauer, S.; Ali, M.; Keshavarz, A. Hydrogen wettability of sandstone reservoirs: implications for hydrogen geo-storage. *Geophys. Res. Lett.* **2021**, *48*, No. e2020GL090814.

(11) Shrestha, P.; Banerjee, R.; Lee, J.; Ge, N.; Muirhead, D.; Liu, H.; Wong, A. K. C.; Ouellette, D.; Zhao, B.; Bazylak, A. Hydrophilic microporous layer coatings for polymer electrolyte membrane fuel cells operating without anode humidification. *J. Power Sources* **2018**, *402*, 468−482.

(12) Zhao, B.; Lee, C. H.; Lee, J. K.; Fahy, K. F.; LaManna, J. M.; Baltic, E.; Jacobson, D. L.; Hussey, D. S.; Bazylak, A. Superhydrophilic porous transport layer enhances efficiency of polymer electrolyte membrane electrolyzers. *Cell Rep. Physical Science* **2021**, *2*, 100580.

(13) Sinton, D. Energy: the microfluidic frontier. *Lab Chip* **2014**, *14*, 3127−3134.

(14) Yun, W.; Ross, C. M.; Roman, S.; Kovscek, A. R. Creation of a dual-porosity and dual-depth micromodel for the study of multiphase flow in complex porous media. *Lab Chip* **2017**, *17*, 1462.

(15) Gupta, A.; Lee, H.; Doyle, P. S. Oil Recovery from Micropatterned Triangular Troughs during a Surfactant Flood. *Langmuir* **2018**, *34*, 10644−10649.

(16) Anbari, A.; Chien, H.-T.; Datta, S. S.; Deng, W.; Weitz, D. A.; Fan, J. Microfluidic model porous media: Fabrication and applications. *Small* **2018**, *14*, 1703575.

(17) Golmohammadi, S.; Ding, Y.; Kuechler, M.; Reuter, D.; Schlueter, S.; Amro, M.; Geistlinger, H. Impact of wettability and gravity on fluid displacement and trapping in representative 2D micromodels of porous media (2D sand analogs). *Water Resour. Res.* **2021**, *57*, 57.

(18) Zhang, Y.; van Nieuwkasteele, J. W.; Qiang, M.; Tsai, P. A.; Lammertink, R. G. H. Spatial Site-Patterning of Wettability in a Microcapillary Tube. *ACS Appl. Mater. Interfaces* **2016**, *8*, 10657−10660.

(19) Silverio, V.; Canane, P. A. G.; Cardoso, S. Surface wettability and stability of chemically modified silicon, glass and polymeric surfaces via room temperature chemical vapor deposition. *Colloids Surf, A Physicochem Eng. Asp* **2019**, *570*, 210−217.

(20) Hu, R.; Wan, J.; Kim, Y.; Tokunaga, T. K. Wettability impact on supercritical CO2 capillary trapping: Pore-scale visualization and quantification. *Water Resour. Res.* **2017**, *53*, 6377−6394.

(21) Davies, R. T.; Kim, D.; Park, J. Formation of liposomes using a 3D flow focusing microfluidic device with spatially patterned wettability by corona discharge. *J. Micromech Microeng* **2012**, *22*, 055003.

(22) Tan, S. H.; Nguyen, N. T.; Chua, Y. C.; Kang, T. G. Oxygen plasma treatment for reducing hydrophobicity of a sealed poly-dimethylsiloxane microchannel. *Biomicrofluidics* **2010**, *4*, 032204.

(23) Abate, A. R.; Krummel, A. T.; Lee, D.; Marquez, M.; Holtze, C.; Weitz, D. A. Photoreactive coating for high-contrast spatial patterning of microfluidic device wettability. *Lab Chip* **2008**, *8*, 2157−2160.

(24) Abate, A. R.; Thiele, J.; Weinhart, M.; Weitz, D. A. Patterning microfluidic device wettability using flow confinement. *Lab Chip* **2010**, *10*, 1774−1776.

(25) Levaché, B.; Azioune, A.; Bourrel, M.; Studer, V.; Bartolo, D. Engineering the surface properties of microfluidic stickers. *Lab Chip* **2012**, *12*, 3028−3031.

(26) Zhao, B.; MacMinn, C. W.; Juanes, R. Wettability control on multiphase flow in patterned microfluidics. *Proc. Natl. Acad. Sci. U.S.A.* **2016**, *113*, 10251−10256.

(27) Odier, C.; Levaché, B.; Santanach-Carreras, E.; Bartolo, D. Forced Imbibition in Porous Media: A Fourfold Scenario. *Phys. Rev. Lett.* **2017**, *119*, 208005.

(28) Irannezhad, A.; Primkulov, B. K.; Juanes, R.; Zhao, B. Fluid-fluid displacement in mixed-wet porous media. *Phys. Rev. Fluids* **2023**, *8*, L012301.

(29) Bartolo, D.; Degre, G.; Nghe, P.; Studer, V. Microfluidic stickers. *Lab Chip* **2008**, *8*, 274−279.

(30) Sollier, E.; Murray, C.; Maoddi, P.; Di Carlo, D. Rapid prototyping polymers for microfluidic devices and high pressure injections. *Lab Chip* **2011**, *11*, 3752−3765.

(31) Geczy, R.; Sticker, D.; Bovet, N.; Häfeli, U.; Kutter, J. P. Chloroform compatible, thiol-ene based replica molded micro chemical devices as an alternative to glass microfluidic chips. *Lab Chip* **2019**, *19*, 798−806.

(32) Chao, C.; Xu, G.; Fan, X. Effect of surface tension, viscosity, pore geometry and pore contact angle on effective pore throat. *Chem. Eng. Sci.* **2019**, *197*, 269−279.

(33) Gu, H.; Duits, M.; Mugele, F. A hybrid microfluidic chip with electrowetting functionality using ultraviolet (UV)-curable polymer. *Lab Chip* **2010**, *10*, 1550−1556.

(34) Wägli, P.; Homsy, A.; de Rooij, N. F. Norland optical adhesive (NOA81) microchannels with adjustable wetting behavior and high chemical resistance against a range of mid-infrared-transparent organic solvents. *Sens. Actuators B Chem.* **2011**, *156*, 994−1001.

(35) Levaché, B.; Bartolo, D. Revisiting the Saffman-Taylor experiment: Imbibition patterns and liquid-entrainment transitions. *Phys. Rev. Lett.* **2014**, *113*, 044501.

(36) Xiao, S.; Zeng, Y.; Vavra, E. D.; He, P.; Puerto, M.; Hirasaki, G. J.; Biswal, S. L. Destabilization, propagation, and generation of surfactant-stabilized foam during crude oil displacement in heterogeneous model porous media. *Langmuir* **2018**, *34*, 739−749.

(37) Moonen, E.; Luttge, R.; Frimat, J.-P. Single cell trapping by capillary pumping using NOA81 replica moulded stencils. *Microelectron. Eng.* **2018**, *197*, 1−7.

(38) Vavra, E.; Puerto, M.; Biswal, S. L.; Hirasaki, G. J. A systematic approach to alkaline-surfactant-foam flooding of heavy oil: microfluidic assessment with a novel phase-behavior viscosity map. *Sci. Rep.* **2020**, *10*, 12930.

(39) Bajgiran, K. R.; Hymel, H. C.; Sombolestani, S.; Dante, N.; Safa, N.; Dorman, J. A.; Rao, D.; Melvin, A. T. Fluorescent visualization of oil displacement in a microfluidic device for enhanced oil recovery applications. *Analyst* **2021**, *146*, 6746−6752.

(40) Watts, J. F.; Wolstenholme, J. *An Introduction to Surface Analysis by XPS and AES*; John Wiley & Sons, 2019.

(41) Luthin, J.; Linsmeier, C. Carbon films and carbide formation on tungsten. *Surf. Sci.* **2000**, *454*, 78−82.

(42) Beamson, G.; Briggs, D. *High Resolution XPS of Organic Polymers: The Scienta ESCA300 Database*; Wiley, 1992.

(43) *NIST X-ray Photoelectron Spectroscopy Database*; NIST Standard Reference Database Number 20; National Institute of Standards and Technology: Gaithersburg, MD, 2000; DOI: 10.18434/T4T88K (accessed Dec 29, 2022).

(44) X-ray Photoelectron Spectroscopy (XPS) Reference Pages. http://www.xpsfitting.com/2014/04/organic-sulphur.html (accessed Dec 29, 2022).

(45) Worley, C. G.; Linton, R. W. Removing sulfur from gold using ultraviolet/ozone cleaning. *J. Vac. Sci. Technol. A: Vac. Surf. Films* **1995**, *13*, 2281−2284.

(46) Xie, A.; Wang, B.; Chen, X.; Wang, Y.; Wang, Y.; Zhu, X.; Xing, T.; Chen, G. Facile fabrication of superhydrophobic polyester fabric based on rapid oxidation polymerization of dopamine for oil−water separation. *RSC Adv.* **2021**, *11*, 26992−27002.

(47) Mathieson, I.; Bradley, R. H. Improved adhesion to polymers by UV/ozone surface oxidation. International journal of adhesion and adhesives. *Int. J. Adhes Adhes* **1996**, *16*, 29−31.

(48) Ederer, J.; Janoš, P.; Ecorchard, P.; Tolasz, J.; Štengl, V.; Beneš, H.; Perchacz, M.; Pop-Georgievski, O. Determination of amino groups on functionalized graphene oxide for polyurethane nanomaterials: XPS quantitation vs. functional speciation. *RSC Adv.* **2017**, *7*, 12464−12473.

(49) Truica-Marasescu, F.; Wertheimer, M. R. Vacuum ultraviolet-induced photochemical nitriding of polyolefin surfaces. *J. Appl. Polym. Sci.* **2004**, *91*, 3886−3898.

(50) Jackson, J. M.; Witek, M. A.; Hupert, M. L.; Brady, C.; Pullagurla, S.; Kamande, J.; Aufforth, R. D.; Tignanelli, C. J.; Torphy, R. J.; Yeh, J. J.; Soper, S. A. UV activation of polymeric high aspect

ratio microstructures: ramifications in antibody surface loading for circulating tumor cell selection. *Lab Chip* **2014**, *14*, 106−117.

(51) Yang, W.; Brownlow, J. W.; Walker, D. L.; Lu, J. Effect of Surfactant-Assisted Wettability Alteration on Immiscible Displacement: A Microfluidic Study. *Water Resour. Res.* **2021**, *57*, e2020WR029522.

(52) Kaminsky, R.; Radke, C. J. Asphaltenes, water films, and wettability reversal. *SPE Journal* **1997**, *2*, 485−493.

(53) Maria, M. S.; Rakesh, P. E.; Chandra, T. S.; Sen, A. K. Capillary flow-driven microfluidic device with wettability gradient and sedimentation effects for blood plasma separation. *Sci. Rep.* **2017**, *7*, 43457.

(54) Liu, C.; Sun, J.; Li, J.; Xiang, C.; Che, L.; Wang, Z.; Zhou, X. Long-range spontaneous droplet self-propulsion on wettability gradient surfaces. *Sci. Rep.* **2017**, *7*, 7552.

(55) Qi, L.; Niu, Y.; Ruck, C.; Zhao, Y. Mechanical-activated digital microfluidics with gradient surface wettability. *Lab Chip* **2019**, *19*, 223−232.

(56) Måløy, K. J.; Furuberg, L.; Feder, J.; Jossang, T. Dynamics of slow drainage in porous media. *Phys. Rev. Lett.* **1992**, *68*, 2161−2164.

(57) Måløy, K. J.; Feder, J.; Jossang, T. Viscous fingering fractals in porous media. *Phys. Rev. Lett.* **1985**, *55*, 2688−2691.

(58) Holtzman, R.; Szulczewski, M. L.; Juanes, R. Capillary fracturing in granular media. *Phys. Rev. Lett.* **2012**, *108*, 264504.

(59) Trojer, M.; Szulczewski, M. L.; Juanes, R. Stabilizing fluid-fluid displacements in porous media through wettability alteration. *Phys. Rev. Applied* **2015**, *3*, 054008.

(60) Datta, S. S.; Chiang, H.; Ramakrishnan, T. S.; Weitz, D. A. Spatial fluctuations of fluid velocities in flow through a three-dimensional porous medium. *Phys. Rev. Lett.* **2013**, *111*, 064501.

(61) Datta, S. S.; Ramakrishnan, T. S.; Weitz, D. A. Mobilization of a trapped non-wetting fluid from a three-dimensional porous medium. *Phys. Fluids* **2014**, *26*, 022002.

(62) Singh, K.; Scholl, H.; Brinkmann, M.; Michiel, M. D.; Scheel, M.; Herminghaus, S.; Seemann, R. The role of local instabilities in fluid invasion into permeable media. *Sci. Rep.* **2017**, *7*, 444.

(63) Utada, A. S.; Fernandez-Nieves, A.; Stone, H. A.; Weitz, D. A. Dripping to jetting transitions in coflowing liquid streams. *Phys. Rev. Lett.* **2007**, *99*, 094502.

(64) Duncanson, W. J.; Lin, T.; Abate, A. R.; Seiffert, S.; Shah, R. K.; Weitz, D. A. Microfluidic synthesis of advanced microparticles for encapsulation and controlled release. *Lab Chip* **2012**, *12*, 2135−2145.